Raman Microspectrometry as a New Approach to the Investigation of Molecular Recognition in Solids: Chloroform−Cryptophane Complexes

Dominique Cavagnat,*,† Thierry Brotin,‡ Jean-Luc Bruneel,† Jean-Pierre Dutasta,‡ Alain Thozet,§ Monique Perrin,§ and François Guillaume†

Laboratoire de Physico-Chimie Moléculaire, Université de Bordeaux I (UMR CNRS 5803), 351 cours de la Libération, 33405 Talence Cedex, France, Laboratoire de Chimie (UMR CNRS 5182), École Normale Supérieure de Lyon, 46 Allée d'Italie, F-69364 Lyon 07, France, and Reconnaissance et Organisation Moléculaire et Biomoléculaire (UMR CNRS 5078) Université Claude Bernard, 69622 Villeurbanne Cedex, France

Received: November 18, 2003; In Final Form: February 10, 2004

Information about the orientation and dynamics of a chloroform molecule encaged in cryptophane-A and cryptophane-E is obtained by means of Raman microspectrometry. The microscopy technique allows us to study the two observed crystalline structures of the $CDCl_3$−cryptophane-A complexes separately. The spectra, recorded under different polarization conditions, are compared with those of $CHCl_3$−D_{30}−cryptophane-A and analyzed in light of the crystalline structures determined by X-ray diffraction. The spectral analysis is improved by ab initio calculations performed for the isolated guest and host molecules. The orientation of the encaged chloroform with the C−H bond pointing toward the center of the cyclotriveratrylene structures is confirmed. The νCD (or νCH) stretching wavenumber of chloroform is red shifted upon complexation as compared to the wavenumber of the gaseous isolated state. This red shift, larger for the $CDCl_3$−cryptophane-E complex than for the $CDCl_3$−cryptophane-A complex, is the signature of stronger binding host−guest interactions with cryptophane-E. In addition, the analysis of the band shape of the νCD stretching vibration of chloroform suggests different rotational dynamics for the guest molecule encaged in cryptophane-A or in cryptophane-E. This work illustrates the capability of the Raman microspectrometry technique to investigate molecular recognition phenomena in solids.

Introduction

Among molecular hosts possessing large 3D cavities, the cryptophanes occupy a particular place because of their high binding properties toward small neutral guest molecules such as chloroform, dichloromethane, or methane.[1−8] Cryptophane molecules are globularly shaped with two cyclotriveratrylene (CTV) units connected by three ethyl or propyl linkers for cryptophane-A and cryptophane-E, respectively. The rigid bowl-shape structure of the cavity of cryptophanes makes these molecules very attractive to the investigation of host−guest interactions. The cryptophane complexes are structurally well-defined assemblies of two neutral species noncovalently bound to each other. These systems are reversibly formed, and their stability depends on several factors. Many questions have been raised about the determination of the binding selectivity and the intracavity arrangement

Because of its rapid development in the last few decades combined with its high selectivity, NMR spectroscopy has been extensively used to study the binding properties of a large range of supramolecular systems. The binding properties of the $CHCl_3$−cryptophane complexes in solution have been evaluated by several NMR studies, leading to the conclusion that cryptophane-A moderately complexes $CHCl_3$ with a somewhat larger binding constant with cryptophane-E.[4−8] The crystal structure of the $CHCl_3$−cryptophane-E complexes has revealed that the chlorine atoms of the encaged chloroform molecule are in the equatorial plane of the cavity whereas the H atom points toward one of the CTV units.[2] The NMR investigation of the rotational mobility of the guest in the cryptophane-E complexes reveals no fast large-scale motion of chloroform inside the cavity.[7,8]

Quite surprisingly, vibrational spectroscopic techniques have not been so intensively used to study molecular recognition phenomena. Most of the work published on this topic concerns vibrational studies of organic compounds encapsulated in zeolites and related materials.[9−11] This is certainly due to difficulties in obtaining infrared or Raman spectra of highly dilute solutions or of crystals of micrometer size. However, because of the considerable technological and computational progress made during these past decades, vibrational spectroscopic techniques have increased in precision and sensitivity and are now able to furnish useful information about such relatively complex organic host−guest systems. For instance, Raman spectrometry, coupled to optical microscope devices, offers a unique way to analyze samples with exceptional spatial resolution (micrometer scale). This technique has proved its efficiency in several applications, such as studies of microcrystalline compounds, surface cartographies, or in-situ analyses of compounds included in transparent matrices.[12,13] However, to our knowledge, Raman microspectrometry has never been used to investigate the interaction of a neutral guest molecule confined in the cavity of a host molecule.

From this point of view, the $CHCl_3$−cryptophane complexes appear to be interesting molecular model systems to test the

* Corresponding author. E-mail: d.cavagnat@lpcm.u-bordeaux1.fr.
† Université de Bordeaux I.
‡ École Normale Supérieure de Lyon.
§ Reconnaissance et Organisation Moléculaire et Biomoléculaire Université Claude Bernard.

10.1021/jp0375158 CCC: $27.50
Published on Web 04/09/2004

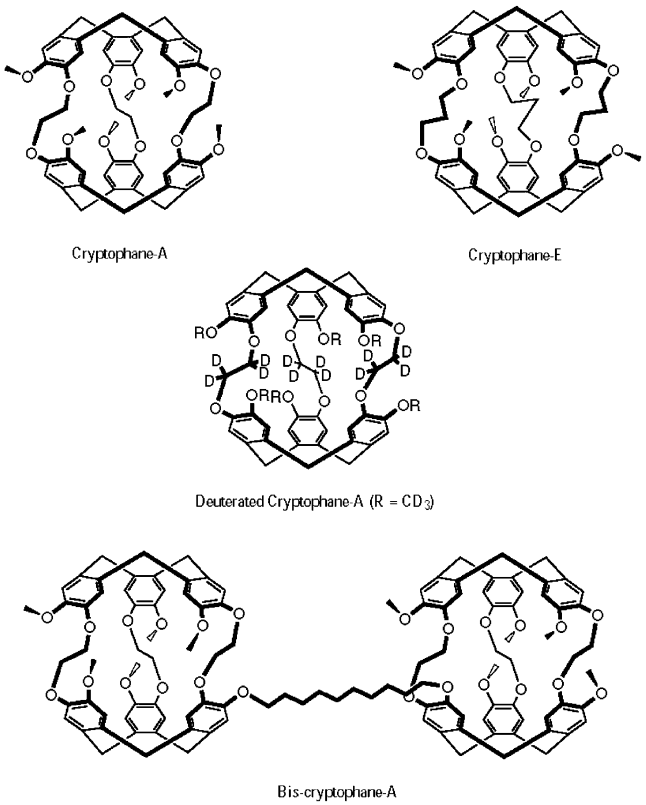

Figure 1. Scheme of a cryptophane-A molecule, a selectively deuterated cryptophane-A molecule, a cryptophane-E molecule, and a bis-cryptophane-A molecule.

ability of Raman microspectrometry to investigate recognition phenomena. As suggested in previous work,[7] the stability of such complexes implies strong anisotropic (directional) interactions between the CTV unit of the host and the H atom of the guest. Many IR and Raman scattering spectroscopic studies completed by theoretical calculations have demonstrated that the isolated CH stretching vibration (present in chloroform) is a very efficient probe of its environment.[14−16] Very small perturbations of this vibration result in important shifts of its wavenumbers. (A difference of 0.001 Å in bond length results in a 10−15-cm^{-1} difference in the stretching wavenumber.) Thus, an observed wavenumber shift of the CH stretching for the encaged chloroform molecule compared to its value in the liquid or in the gas phase would be characteristic of host−guest interactions.

In this study, the presence of numerous ν_{C-H} stretching vibration bands due to the cryptophane cavity would completely mask the ν_{C-H} stretching line of $CHCl_3$. Thus, despite the lesser sensitivity of the CD bond compared to that of the CH bond (by a factor of about 1.35), we have used deuterated chloroform. The ν_{C-D} stretching appears in a spectral window (2000−2500 cm^{-1}) where no other bands are expected. Some experiments have nevertheless been performed with $CHCl_3$ complexed with the selectively deuterated cryptophane-A shown in Figure 1.

In this paper, we present a polarized Raman microspectrometry study of microcrystals of cryptophane-A, selectively deuterated cryptophane-A, bis-cryptophane-A, and cryptophane-E (Figure 1) encapsulating chloroform molecules. Thanks to the micrometer spatial resolution provided by the Raman microspectrometer, monocrystalline entities have been isolated. The crystallographic structures of these different entities were determined by X-ray diffraction analysis. Ab initio calculations of the isolated empty cryptophane-A unit were also realized.

Experimental Section

Materials. Cryptophane-A and -E were synthesized from a multistep synthesis using the template method.[17] The syntheses of the selectively deuterated molecule[18] and the bis-cryptophane[19] were described previously.

All of the compounds (except bis-cryptophane-A) were purified twice by column chromatography on silica gel and then recrystallized from a mixture of chloroform and ethanol. Bis-cryptophane-A was purified twice on silica gel following the method reported in the literature.[20]

Cryptophane-A and -E were first dissolved in deuterated chloroform (purchased from Aldrich). A small amount of ethanol was then added. Small single crystals of the complexes were obtained by slow evaporation of the solutions at room temperature.

Crystallographic Measurements. X-ray data were collected at 173 K on a Nonius Kappa CCD diffractometer at the Centre de Diffractométrie Henri Longchambon using Mo Kα radiation ($\lambda = 0.71069$ Å). The initial set of cell parameters was obtained for each crystallographic form from 10 frames with 1° steps. All of the reflections were used in refinement after merging. The structures were solved by direct methods and refined by least-squares methods using SHELXS and SHELXL, respectively.[21] Crystal data and refinement parameters are reported in Table 1.

Raman Scattering. The Raman spectra were recorded with a Lab Ram II spectrometer (Jobin Yvon) using excitation radiation (wavelength of 514.5 Å) provided by an argon−krypton ion laser (Spectra Physics). The power of the incident laser beam was sufficiently low (typically around 2 mW on the sample) to avoid damaging the crystals. The spectral instrumental resolution was on average 2 cm^{-1} (hwhh) (1800-line grating). The microscopic measurements were performed using a microscope with a ×50 ULWD objective. The low-temperature spectra were obtained with a THMS600 temperature stage (LINKAM) cooled with liquid nitrogen.

Because we are studying single crystals, we define a laboratory reference frame where the *y* axis is collinear to the propagation direction of the incident light, perpendicular to the plane that contains the *x* and *z* axes. The incident laser light could be polarized vertically (V ⇔ defining the *z* axis) or horizontally (H ⇔ defining the *x* axis). The scattered light was collected in the same direction as that of the incident light (backscattering) and analyzed through a polarizer along its V (*z*) or H (*x*) components. Thus, four spectra for each sample with polarization conditions written in Porto notation[22] as $y(zz)\bar{y}$, $y(zx)\bar{y}$, $y(xx)\bar{y}$, and $y(xz)\bar{y}$ could be obtained.

Computational Methodology. The minimum-energy structure of the cryptophane-A cage was recently calculated in the case of the xenon−cryptophane-A complexes by using a density functional method (B3LYP functional) and a 6-311G** basis set.[23] In this work, the gauche conformation of the $O-CH_2-CH_2-O$ linkers was retained to be consistent with the SPINOE experiments.[5] The geometry optimization was carried out only for a fragment representing two-thirds of the cage. The whole cage was then generated from this fragment.

In the present work, we need to calculate the vibrational frequencies of the cryptophane-A−chloroform complexes. Owing to the large atomic size of this system, we have assumed that most of the vibrational modes of the cryptophane-A cage were only slightly perturbed by the chloroform guest. Thus, the minimum-energy structure of the whole empty cryptophane-A cage was calculated at the HF level with a 6-31G* basis set by the following method. First, we optimized one-third of the CTV

TABLE 1: Data and Refinement Parameters for the $CHCl_3$−Cryptophane Complexes

	polyhedral crystals	rhomb crystals	rod crystals
formula	$C_{57.5}H_{57.5}Cl_{10.5}O_{12}$	$C_{55}H_{55}Cl_3O_{12}$	$C_{56}H_{56}Cl_6O_{12}$
formula wt	1312.76	1014.34	1133.71
crystal system	monoclinic	monoclinic	monoclinic
space group	$P2_1/n$	$P2_1/c$	$P2_1/n$
a (Å)	20.445(4)	22.284(5)	13.383(3)
b (Å)	12.771(3)	11.275(2)	21.935(4)
c (Å)	23.271(5)	20.613(4)	17.901(4)
α (deg)	90.00	90.00	90.00
β (deg)	96.05(3)	114.60(3)	95.09(3)
γ (deg)	90.00	90.00	90.00
V (Å^3)	6042(2)	4708.8(16)	5233.9(18)
T (K)	173	173	173
D_x (g cm^{-3})	1.443	1.431	1.439
Z	4	4	4
F(000)	2708	2128	2360
μ (mm^{-1})	0.543	0.263	0.393
crystal size (mm)	0.75 × 0.30 × 0.30	0.20 × 0.20 × 0.05	0.50 × 0.10 × 0.04
$2\theta_{max}$ (deg)	45.4	45.5	40.6
range of hkl	$-22 \le h \le 22$	$-24 \le h \le 24$	$-12 \le h \le 12$
	$-9 \le k \le 13$	$-12 \le k \le 11$	$-21 \le k \le 20$
	$-25 \le l \le 25$	$-22 \le l \le 22$	$-17 \le l \le 17$
no. of collected reflns	11011	10203	16670
no. of unique reflns	7577	6233	5034
no. of observed reflns	3668		
[$I \ge 2\sigma(I)$]		3414	2874
no. of parameters	757	620	673
no. of restraints	53	6	0
goodness of fit	1.037	1.875	0.937
R (R all data)	0.1027(0.1992)	0.1668 (0.2489)	0.0649 (0.1345)
WR2	0.2692	0.4633	0.158

TABLE 2: C−D and C−H Stretching Wave Numbers (cm^{-1}) Observed for Pure $CDCl_3$ and $CHCl_3$ in Liquid and Gas Phases and for Guest $CDCl_3$ and $CHCl_3$ in Cryptophane-A or -E Complex Crystals

	$CDCl_3$ $CHCl_3$ liquid	$CDCl_3$ $CHCl_3$ gas	cryptophane-A (rods)	cryptophane-A (rhomb)	bis-cryptophane-A	cryptophane-E
			2259 ± 2			
ν(C−D)	2255	2265	2247 ± 2	2245 ± 2	2246 ± 2	2235 ± 2
ν(C−H)	3020	3033		3005 ± 2[a]		

[a] Selectively deuterated cryptophane-A.

unit. Then the C_3 symmetry operations generated the CTV bowl. This structure was also optimized at the HF level with a 6-31G* basis set. Then we introduced the $-OCH_2CH_2O-$ between the two optimized CTV units by constraining the D_3 symmetry of cryptophane-A. This symmetry constraint generates an anti conformation of the $O-CH_2-CH_2-O$ linkers, as mostly found for the cryptophane-A−chloroform complexes.[4,17] With this symmetry constraint, we could achieve a quantum calculation for the whole empty cage at the HF level with a 6-31G* basis set that constitutes 1098 basis functions.

The molecular geometry of chloroform was optimized with the Gaussian 98 program[24] at the HF level with a 6-31G** basis set that constitutes 77 basis functions.

Vibrational wavenumbers were calculated numerically by determining second derivatives of energy with respect to geometry distortions. For comparison with the experimental values, the calculated ones were scaled by the usual factor (∼0.9). The components of the polarizability tensor corresponding to the CH stretching vibrations were calculated from the ab initio-computed atomic polar tensors.[25,26] More complete and searching calculations of this system are in progress.[27]

Results and Discussion

I. $CDCl_3$−Cryptophane-A Complexes. *1. Crystallographic Structure.* Because of the difficulties encountered in obtaining single crystals of good optical quality, the X-ray crystallographic structures of $CHCl_3$−cryptophane-A complexes have been determined only recently and are described in this paper. Three polymorph structures of this complex, exhibiting different crystal morphologies, have been observed (Table 1).

a. Rhomb Crystals. Single crystals displaying rhomblike morphology are the most common ones obtained when preparing $CHCl_3$−cryptophane-A complexes in the presence of ethanol. The unit cell of these crystals, shown in Figure 2, is monoclinic with space group $P2_1/c$ (a = 22.284 Å, b = 11.275 Å, c = 20.613 Å, and β = 114.6°) and four $CHCl_3$−cryptophane-A complexes per unit cell (V = 4709 Å^3) (Table 1). In the rhomb crystal, there is one encaged chloroform in each cryptophane-A cavity. The chlorine atoms of each encaged chloroform occupy the central equatorial plane of the host, and the C−H bond is collinear to the C_3 axis of the cryptophane molecule. In this structure, the projections versus the monoclinic b axis (one of the optical axes) of all of the C_3 axes of the $CHCl_3$−cryptophane-A molecules are parallel to the same direction that is tilted by only 9° versus the principal diagonal of the *ac* plane of the monoclinic lattice.

b. Rod Crystals. Single crystals with rodlike morphology are quite often observed but are not stable under ambient conditions and become powder after a few days. The unit cell of these crystals, shown in Figure 3, is also monoclinic with space group $P2_1/n$ (a = 13.383 Å, b = 21.935 Å, c = 17.901, Å and β = 95.09°) and four $CHCl_3$−cryptophane-A molecules per unit cell (V = 5234 Å^3) (Table 1). This structure is more complex than that of the rhomb crystal because additional interstitial chloro-

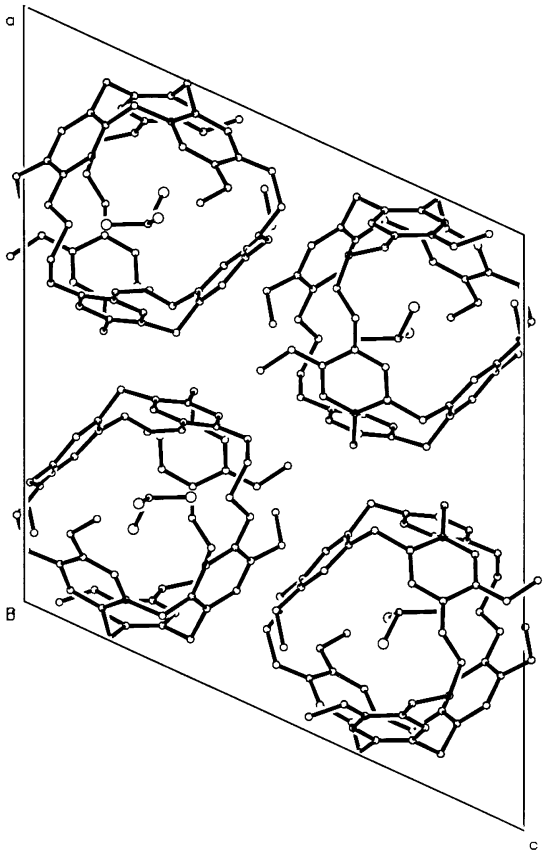

Figure 2. X-ray structure of rhomb crystals of the $CHCl_3$−cryptophane-A complex (*ac* plane projection of the unit cell, H atoms not displayed).

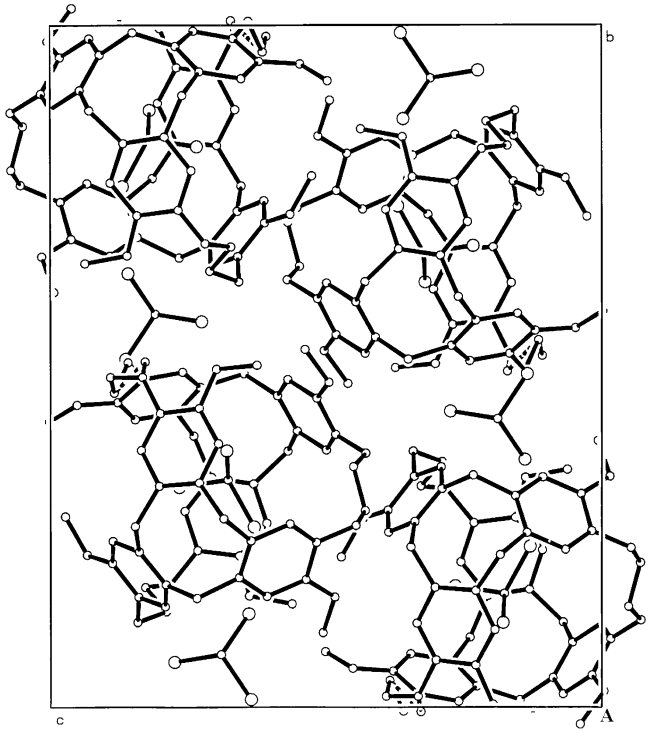

Figure 3. X-ray structure of rod crystals of the $CHCl_3$−cryptophane-A complex (*bc* plane projection of the unit cell, H atoms not displayed).

form molecules (four per unit cell) are located between the $CHCl_3$−cryptophane-A units. Each C−H bond of the encapsulated chloroform molecule is collinear to the C_3 axis of the cryptophane. The projections in the *ac* plane of the C_3 axes of

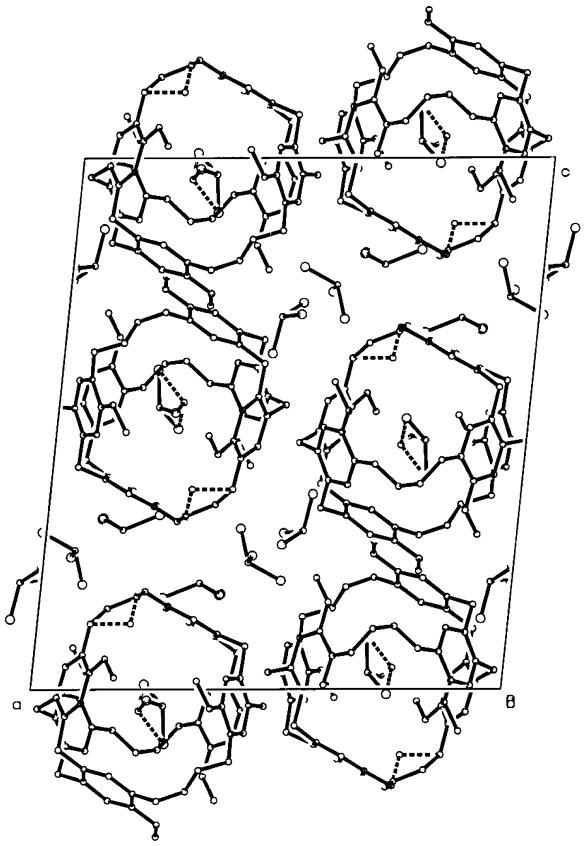

Figure 4. X-ray structure of polyhedral crystals of the $CHCl_3$−cryptophane-A complex (*ac* plane projection of the unit cell, H atoms not displayed).

the $CHCl_3$−cryptophane-A complexes are again parallel to the same direction that makes an angle of 45° with the *a* axis of the monoclinic cell. In the same plan projection, the CH bond of the interstitial chloroform molecules is tilted by only 13° from the *a* axis.

c. Polyhedral Crystals. Despite several attempts to reproduce this result, a third polymorph structure displaying polyhedral morphology has been observed only once. However, we managed to determine its X-ray structure (Figure 4), which is also monoclinic with space group $P2_1/n$ (a = 20.445 Å, b = 12.771 Å, c = 23.271 Å, and β = 96.05°) and four $CHCl_3$−cryptophane-A complexes per unit cell (V = 6042 Å^3) (Table 1). As in the rod crystal, $CHCl_3$−cryptophane-A units coexist with interstitial chloroform molecules (10 per unit cell). All of the C_3 axes of the $CHCl_3$−cryptophane-A complexes are parallel to the same direction (approximately along the principal diagonal of the *ac* plane) whereas the orientations of the CH bond of the interstitial chloroform molecules are different. The presence of numerous interstitial chloroform molecules making the structure very unstable probably explains our difficulties in reproducing these observations.

2. Raman Microscopy Scattering. Because the characteristic shapes of the various single crystals can be easily identified under the microscope, Raman microscopy has been exploited to study separately each single rhomb or rod crystal, the polyhedral structure having never been observed during our Raman scattering experiments.

a. Rhomb Crystals. The well-defined rhomb shape of the single microcrystals (Figure 5) allows us to perform polarized Raman scattering measurements. As described in the Experimental Section, the *y* axis corresponds to the propagation direction of the incident light, and the *x* and *z* axes are defined

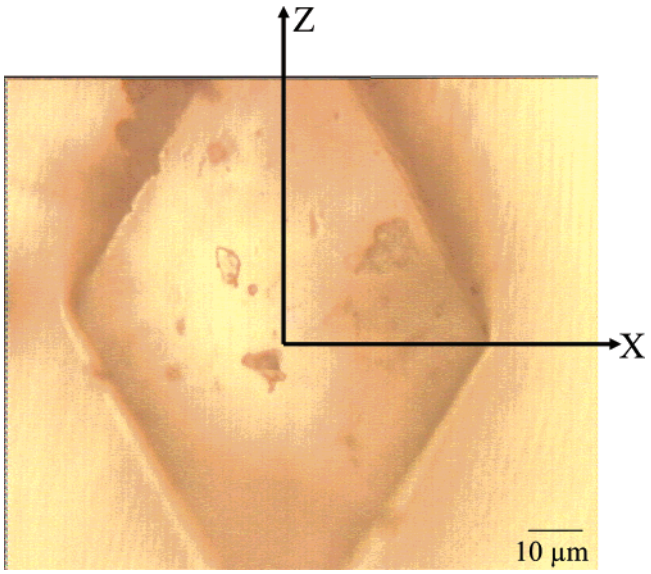

Figure 5. Photography of a rhomb crystal of the $CDCl_3$−cryptophane-A complex with the *z* and *x* laboratory axes.

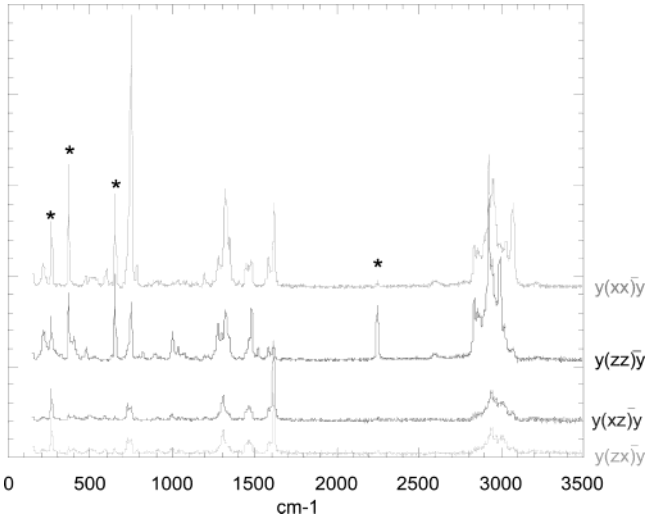

Figure 6. $y(xx)\bar{y}$, $y(zz)\bar{y}$, $y(xz)\bar{y}$, and $y(zx)\bar{y}$ Raman spectra of a rhomb crystal of the $CDCl_3$−cryptophane-A complex. $CDCl_3$ bands are quoted with an asterisk.

as the directions of the diagonals of the rhomb monocrystal (*z* corresponding to the principal axis).

The $y(xz)\bar{y}$ and $y(zx)\bar{y}$ Raman spectra obtained for these rhomb crystals are very similar, and the intensities of most of the observed bands are weak (Figure 6). In contrast, most of the bands in the $y(xx)\bar{y}$ and $y(zz)\bar{y}$ polarizations are intense (Figure 6). Furthermore, we note strong polarization effects when comparing $y(xx)\bar{y}$, $y(zz)\bar{y}$, and $y(xz)\bar{y}$ or $y(zx)\bar{y}$ spectra. This suggests that the *x* and *y* laboratory axes are very close to the optical axes of the single crystal.

To interpret the observed Raman spectra, it is necessary to consider the symmetry properties of the $CDCl_3$−cryptophane-A complex in the crystal. According to the X-ray data, the $CDCl_3$−cryptophane-A complex sits in a general position in the crystal that belongs to the C_{2h} crystallographic symmetry point group. The isolated $CDCl_3$−cryptophane-A unit belongs to the D_3 symmetry group, and the isolated $CDCl_3$ molecule, to the C_{3v} symmetry group.

Thus, as shown below in the correlation diagram, only the A_g or B_g symmetry vibrational modes of the crystal are Raman-active. For vibrational modes with A_g symmetry, only the

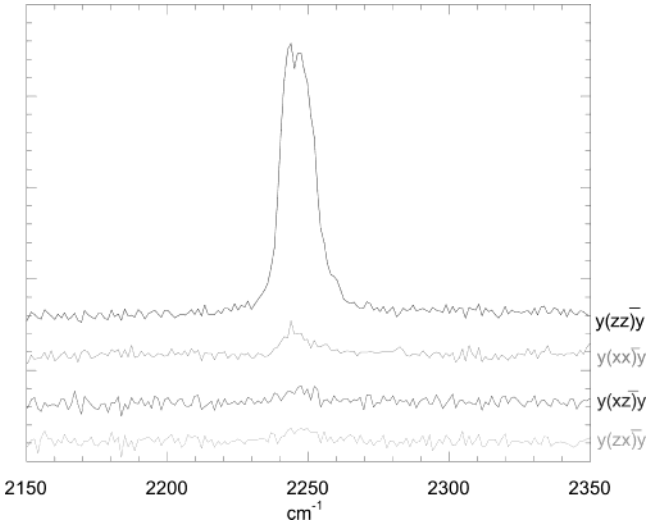

Figure 7. $y(xx)\bar{y}$, $y(zz)\bar{y}$, $y(xz)\bar{y}$, and $y(zx)\bar{y}$ Raman spectra of a rhomb crystal of the $CDCl_3$−cryptophane-A complex in the CD stretching region.

(α'_{xx}, α'_{yy}, α'_{zz}, α'_{zx}) terms of the induced polarizability tensor $\bar{\alpha}'$ are nonzero whereas only the (α'_{zy}, α'_{xy}) terms are nonzero for the vibrations with B_g symmetry. However, the polarization setup of our experiments allows only the observation of the A_g symmetry modes. (See above.)

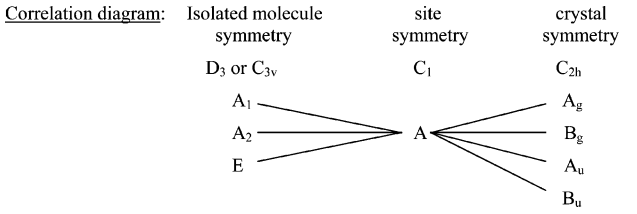

All of the vibrational modes of the encaged deuterated chloroform molecules are expected in the spectral region between 200 and 2500 cm^{-1}. Unfortunately, numerous vibrational bands of the cryptophane units are also expected in this region. Nevertheless, three vibrational modes at 264, 368, and 652 cm^{-1}, not present in the spectrum of the powder "empty" cryptophane-A, can be easily assigned to chloroform molecules (marked with an asterisk in Figure 6). They correspond to the most intense bands of the Raman spectrum of liquid $CDCl_3$ assigned respectively to the $\delta_e CCl_3$ and $\delta_s CCl_3$ bending modes and to the $\nu_s CCl_3$ stretching mode. Their wavenumbers are very similar to those observed in the gas phase (262, 365, and 658 cm^{-1}).[28] The weaker $\nu_e CCl_3$ stretching mode appearing at 747 cm^{-1} in the spectrum of gas chloroform is hidden in the complex by a strong band at 745 cm^{-1} assigned to cryptophane-A. Because of its weak Raman intensity, the $\delta_e CDCl$ bending mode, measured at 915 cm^{-1} in gas chloroform, cannot be observed in the $CDCl_3$−cryptophane-A spectra. In the 2000−2500-cm^{-1} region where only the stretching mode of the C−D bond of chloroform is expected, the $y(zz)\bar{y}$ Raman spectra of the rhomb crystals show a single band located at 2245 ± 2 cm^{-1} (Figures 6 and 7). This wavenumber is significantly lower than that observed in the liquid phase (−10 cm^{-1}) or in the gas phase (−20 cm^{-1}) of $CDCl_3$ (Table 2). (The gas phase is generally considered to be a reference for studying shifts upon complexation.[9]) This red shift of the CD stretch, indicating a softening of the CD bond ($\Delta r_{CH} \approx +2.7 \times 10^{-3}$ Å[14−16]), is characteristic of a specific interaction between the C−D bond of chloroform and one of the two electron-rich CTV units that act as proton acceptors, the $CDCl_3$ being a proton donor.[9,29,30]

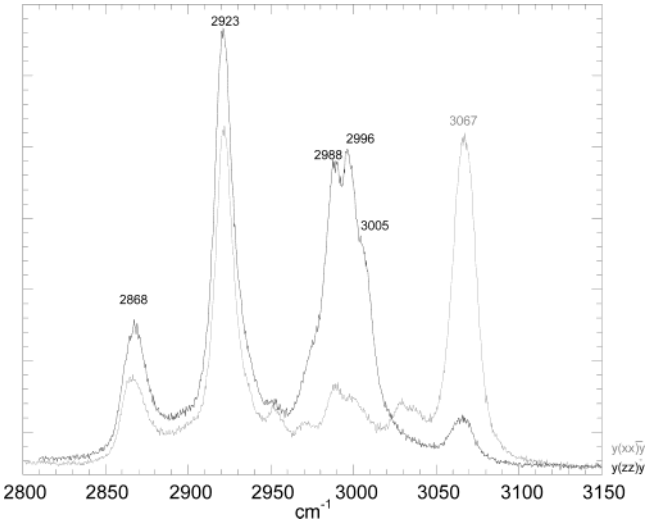

Figure 8. $y(xx)\bar{y}$ and $y(zz)\bar{y}$ Raman spectra of a rhomb crystal of the $CHCl_3$−deuterated cryptophan-A complex in the CH stretching region.

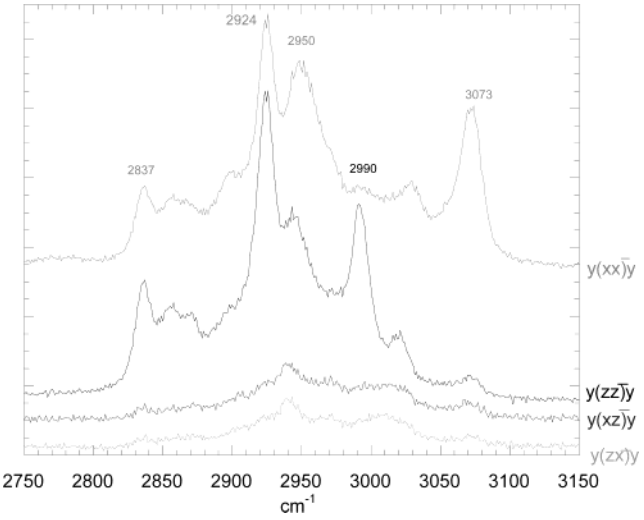

Figure 9. $y(xx)\bar{y}$, $y(zz)\bar{y}$, $y(xz)\bar{y}$, and $y(zx)\bar{y}$ Raman spectra of a rhomb crystal of the $CDCl_3$−cryptophane-A complex in the CH stretching region.

All of the $CDCl_3$ bands are very weak in the $y(xz)\bar{y}$ and $y(zx)\bar{y}$ Raman spectra except that at 264 cm^{-1}, which is assigned to the $\delta_e CCl_3$ bending mode. The intensity variations of the $CDCl_3$ vibrations are not significant between the $y(xx)\bar{y}$ and the $y(zz)\bar{y}$ spectra, excepted those observed for the ν(CD) band at 2245 cm^{-1}. The intensity of this band decreases by a factor higher than 10 from the $y(zz)\bar{y}$ spectrum to the $y(xx)\bar{y}$ one (Figure 7). The polarizability tensor calculated by the ab initio method for the stretching mode in the isolated molecule is diagonal. The value of the α'_{zz} term is much larger than that of the α'_{xx} and α'_{yy} components ($\alpha'_{xx} = \alpha'_{yy} = {}^1/_{16}\ \alpha'_{zz}$), z being collinear to the C_3 symmetry axis of the molecule. This polarization effect demonstrates that the molecular C_3 symmetry axes of chloroform molecules in the unit cell are quasi-collinear to the laboratory z axis. According to the X-ray diffraction data (see above), the angle between the C_3 symmetry axes of the complex units and the principal diagonal of the *ac* plane of the monoclinic lattice is only 9°. Thus, the z laboratory axis corresponds to the diagonal of the *ac* plane of the monoclinic cell as shown schematically in Figure 5. This confirms the orientation of the CD bond in the cryptophane cavity. The $\nu_s CCl_3$ mode should present very similar behavior, but its intensity is almost the same in the $y(xx)\bar{y}$ and the $y(zz)\bar{y}$ spectra (Figure 6). This suggests some donor−acceptor electronic interactions between the chlorine atoms of the encaged chloroform and the cryptophane molecules.[30] The analysis of the spectra obtained with the rhomb crystals of $CHCl_3$-deuterated cryptophane-A confirms these results. As shown in the Figure 8, in the CH stretching region, less embedded by CH stretching bands of the cavity than that of the perhydrogenated derivative, the CH stretching band of the encaged chloroform appears as a shoulder at 3005 cm^{-1} and displays the same polarizability behavior between the $y(xx)\bar{y}$ and the $y(zz)\bar{y}$ spectra. Furthermore, the frequency shift of the CH stretching vibration of $CHCl_3$ (−28 cm^{-1} compared to the gas-phase value) is in good isotopic ratio with that observed for the CD stretching of the deuterated analogue $CDCl_3$ (Table 2).

All of the other bands of the spectra are due to vibrations of the cryptophane-A host molecules (noted as cAh in the following text). In the 2500−3500-cm^{-1} region (Figure 9), numerous C−H stretching vibrations (aromatic, methylene bridges, methoxy groups and ethylene linkers) of cAh are observed. We have largely assessed the assignment of the bands observed in this region by means of ab initio-calculated frequencies even if the molecular structure calculated for the isolated cryptophane molecule is not rigorously similar to that adopted when it encages a chloroform molecule in the crystalline state. In particular, the symmetry constraints lead to an imposed anti−anti conformation for the $-OCH_2CH_2O-$ linkers. However, this linker conformation, which gives the cavity its maximum possible extension (ca. 82 $Å^3$), is well adapted to the guest chloroform size (ca. 72 $Å^3$) and is in agreement with the crystallographic data.[4] The spectra of rhomb crystals of complexes involving the selectively deuterated derivative of cryptophane-A ($(-OCD_3)_6$ and $(-OCD_2CD_2O)_3$) noted as cAd in the following text (Figure 8) have also guided this assignment.

First, we assign the strong band at 3073 cm^{-1} in the cAh $y(xx)\bar{y}$ spectrum (Figure 9) (which appears at 3067 cm^{-1} in the cAd $y(xx)\bar{y}$ spectrum, Figure 8) to the νCH stretching vibrations of the aromatic rings. The α'_{xx} component of the polarizability tensor, calculated for these CH stretching modes, has a much larger value than the α'_{zz} component. This is in good agreement with the quasi-extinctions in the $y(zz)\bar{y}$ spectra of these bands. This demonstrates that these CH bands are nearly perpendicular to the molecular C_3 axis and confirms well the chloroform molecule orientation in the cryptophane cage.

The analysis of the ab initio calculations shows that the two CH bonds of each methylene bridge connecting the phenyl rings are not equivalent. Indeed, the stretching modes of the CH bonds labeled CH_i (pointing toward the interior of the CVT crown) are calculated to be 3000 cm^{-1} (in-phase vibrations) and 2973 cm^{-1} (out-of-phase vibrations) with a α'_{zz} component of the polarizability tensor larger than the α'_{xx} component. They correspond to the bands observed in the Cad spectra at 2996 and 2988 cm^{-1} that display a strong polarization effect (Figure 8). The stretching modes of the CH bonds labeled CH_o (pointing toward the exterior of the CTV crown) are calculated to be 2926 cm^{-1} (in-phase vibrations) and 2924 cm^{-1} (out-of-phase vibrations) with α'_{xx} and α'_{zz} components of the polarizability tensor of the same order of magnitude. They correspond to the band observed in the Cad spectra at 2923 cm^{-1} that exhibits almost the same intensity in the $y(xx)\bar{y}$ and $y(zz)\bar{y}$ spectra (Figure 8). Such a large difference in the CH stretching wavenumbers of the CH_i and the CH_o bonds (ca. 70 cm^{-1}) shows the strong shielding effect of the CTV crowns.

The bending and wagging modes of these methylene groups are calculated to be 1517 cm^{-1} (in-phase vibrations), 1487 cm^{-1}

(out-of-phase vibrations) and 1340 cm^{-1} (in-phase vibrations), 1325 cm^{-1} (out of phase vibrations), respectively. Some Fermi resonance phenomena involving overtone or combination states of these deformation modes can only slightly perturb the CH_o stretching modes owing to the bad frequency matching. Thus, the band observed at 2868 cm^{-1} (Figure 8) is assigned preferably to a combination of the strong aromatic ring vibrations.

These methylene bridge modes are not easily observed in the Cah spectra (Figure 9) at 2990 and 2924 cm^{-1} because they merge in several other vibrational features due to the methyl groups ($-CH_3$) and to the ethylene linkers ($-(CH_2)_2-$). The ν_aCH_2 stretching mode (E symmetry) of the ethylene linkers is calculated to be 2996 cm^{-1} (in-phase vibrations) and 2974 cm^{-1} (out-of-phase vibrations); the ν_sCH_2 stretching mode (A_1 symmetry) is at 2936 cm^{-1} (in-phase vibrations) and 2933 cm^{-1} (out-of-phase vibrations). The bending and wagging vibrations are calculated to be 1477 cm^{-1} (in-phase vibrations), 1468 cm^{-1} (out-of-phase vibrations), and 1420 cm^{-1}. Combination and overtone states of these deformation modes can enter into Fermi resonance with the stretching modes, leading to some splits in the CH stretching bands. Keeping in mind this fact, we can assign the broad features observed at 3022 and 2950 cm^{-1} to these more or less perturbed CH stretching modes.

We calculate the CH stretching modes of the methoxy groups at 2990 cm^{-1} for the ν_aCH_3, 2960 cm^{-1} for the ν'_sCH_3, and 2892 cm^{-1} for the ν_sCH_3; the δ_a, δ'_s, and δ_sCH_3 bending modes are at 1470, 1456, and 1440 cm^{-1}, respectively. These values are in good agreement with those observed and calculated for other related methoxy groups.[31,32] As often observed for the methyl groups, combination and overtone states of the deformation modes are in strong Fermi resonance with the stretching modes. They are responsible for the complex features observed at 2837, 2857, and 2899 cm^{-1} in the Cah spectra (Figure 9) that are not present in the Cad spectra (Figure 8) and enter into the complex spectral features observed between 2940 and 3000 cm^{-1}.

We have investigated the temperature effect on the chloroform C−D stretching Raman spectra in these rhomb crystals. The wavenumber of this mode remains constant, and only a slight narrowing (7−6 cm^{-1} hwhh) is observed when decreasing the temperature from 293 to 93 K. This is consistent with all of the previously collected data supporting the idea that the C−D bond is highly ordered along the C_3 axis of cryptophane-A and that it experiences no fast motion in the cavity.

b. Rod Crystals. The microcrystals belonging to the second polymorph structure exhibit rodlike morphology. The propagation direction of the incident light again defines the *y* axis; the length and the width of the rod monocrystals define the *z* and *x* axes, respectively.

The spectra of these rod crystals display features quite similar to those of the rhomb crystals but with fewer cutoff polarization effects, showing that the laboratory axes do not correspond exactly to the optical axes (Figure 10).

The most characteristic difference between these spectra and those of the rhomb crystals appears in the νCD region that exhibits two distinct signals at 2247 and 2259 cm^{-1} (−18 and −6 cm^{-1}, respectively, compared to the signals of gaseous chloroform) (Figure 11, Table 2). Referring to the X-ray crystallographic structure of this polymorph form and by analogy to the Raman spectra of the rhomb crystals, the band at 2247 cm^{-1} is assigned to the νCD mode of chloroform encapsulated in the cryptophane-A cavity; the other one at 2259 cm^{-1} is assigned to the νCD mode of the interstitial chloroform molecules present in this structure. The detection of the signal

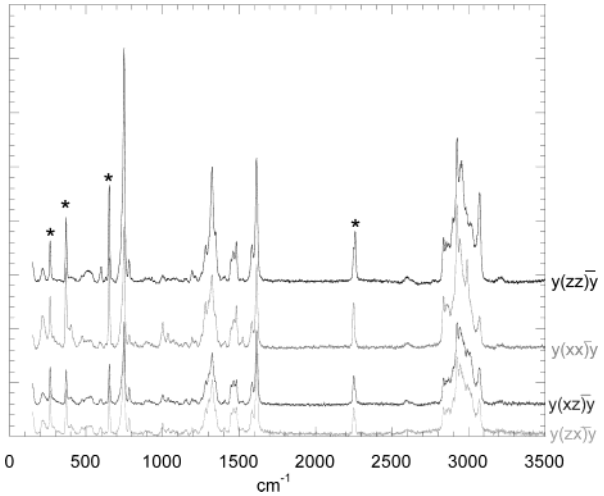

Figure 10. $y(xx)\bar{y}$, $y(zz)\bar{y}$, $y(xz)\bar{y}$, and $y(zx)\bar{y}$ Raman spectra of a rod crystal of the $CDCl_3$−cryptophane-A complex. $CDCl_3$ bands are noted with an asterisk

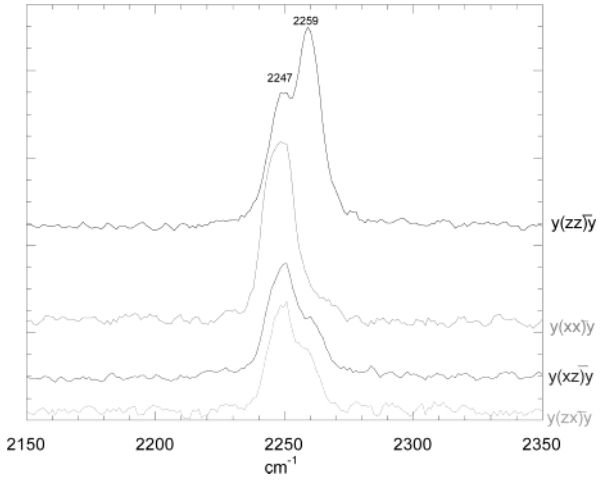

Figure 11. $y(xx)\bar{y}$, $y(zz)\bar{y}$, $y(xz)\bar{y}$, and $y(zx)\bar{y}$ Raman spectra of a rod crystal of the $CDCl_3$−cryptophane-A complex in the CD stretching region.

corresponding to interstitial chloroform demonstrates the sensitivity of the technique to the discrimination of the environment of the guest molecules, which is expected to be significantly different for the encaged and interstitial chloroform molecules. Furthermore, the quasi-extinction of the band at 2259 cm^{-1} in the $y(xx)\bar{y}$ spectrum indicates that the CD bonds of the interstitial chloroform molecules have different orientations compared to those of the encaged ones. Comparisons between the polarized spectra in the CH and CD stretching regions for cryptophane and encaged chloroform lead to conclusions similar to those obtained for the rhomb crystals.

The temperature dependence of the νCD vibrations in the rod crystals is displayed in Figure 12. With decreasing temperature, as observed for rhomb crystals, the wavenumber of the νCD vibration of the encaged chloroform exhibits no change. On the contrary, the second peak assigned to the interstitial chloroform molecules shifts toward higher wavenumbers (+6.5 cm^{-1} from 293 to 93 K). This suggests a reorganization of interstitial chloroform molecules in the lattice and is consistent with the fact that interstitial chloroform molecules interact only weakly with cryptophane.

c. $CDCl_3$−Bis-cryptophane-A. Preliminary Raman scattering experiments on the $CDCl_3$−bis-cryptophane-A complex have also been performed. This molecule (Figure 1) is made of two

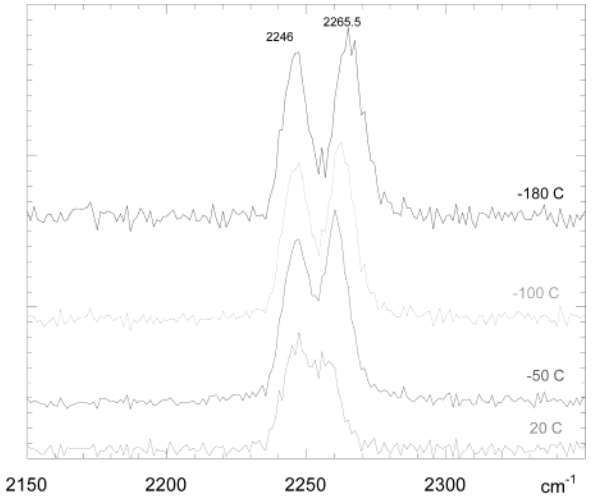

Figure 12. Temperature effect on the Raman spectra of a rod crystal of the $CDCl_3$−cryptophane-A complex in the CD stretching region.

cryptophane-A units connected by an alkyl chain. We never succeeded in determining the crystallographic structure of this complex because of the difficulties in preparing single crystals of good quality, which is not surprising because of the presence of the long alkyl chain and several diastereoisomeric species. Raman spectra of small crystals with no easily defined shape show the presence of a single peak in the νCD stretching region at 2246 cm^{-1}, a value very similar to that observed in the previous measurements for the encaged chloroform in the $CDCl_3$−cryptophane-A complexes (Table 2). In these crystals, all chloroform molecules are encaged in the cryptophane cavities.

II. $CDCl_3$−Cryptophane-E Complexes. Only one form of the $CHCl_3$−cryptophane-E crystals has been previously observed by means of X-ray diffraction. The crystalline structure is monoclinic with space group $P2_1/c$ (a = 38.262 Å, b = 12.441 Å, c = 12.748 Å, and β = 95.78°) and four $CHCl_3$−cryptophane-E complexes per unit cell (V = 6037 $Å^3$).[2] In the crystal, there is one encaged chloroform in each cryptophane-E cavity. As already observed with cryptophane-A, the C−H bond of chloroform points either up or down along the C_3 axis of the cryptophane cavity.

All of the crystals that we have observed under the microscope display the same hexagonal morphology (Figure 13). We failed to determine optical axes from the observed polarization effects. The spectra of these crystals exhibit features similar to those observed for the $CDCl_3$−cryptophane-A complex (Figure 14). The νCH stretching spectral region assignment is quite similar to that of cryptophane-A (Figure 15). However, the presence of an additional CH_2 group in the three linkers connecting the CTV units ($-(CH_2)_3-$ in cryptophane-E instead of $-(CH_2)_2-$ in cryptophane-A) leads to more embedded spectral features with intense bands at 2875, 2936, 2953, and 3017 cm^{-1}. Ab initio calculations are in progress to confirm the assignment of all of the observed bands.

The Raman spectra in the νCD stretching region display a single peak at 2235 cm^{-1} (Figure 16). This red shift (-30 ± 2 cm^{-1} compared to that of gaseous $CDCl_3$) is larger than that observed for the $CDCl_3$−cryptophane-A complexes (Table 2). This suggests a larger softening of the CD bond ($\Delta r_{CH} \approx +4 \times 10^{-3}$ Å) characteristic of a stronger attractive interaction between the host cryptophane-E and the guest chloroform. Furthermore, the width of this band is twice as narrow as that observed in the case of $DCCl_3$−cryptophane-A complexes (2.5-cm^{-1} hwhh compared to 7-cm^{-1} hwhh at 293 K). When the temperature decreases, we observe a small shift toward low frequency (-2 cm^{-1} from 293 to 93 K) and a narrowing of the band (2.5-cm^{-1} hwhh at 293 K, 2.0-cm^{-1} hwhh at 93 K). This

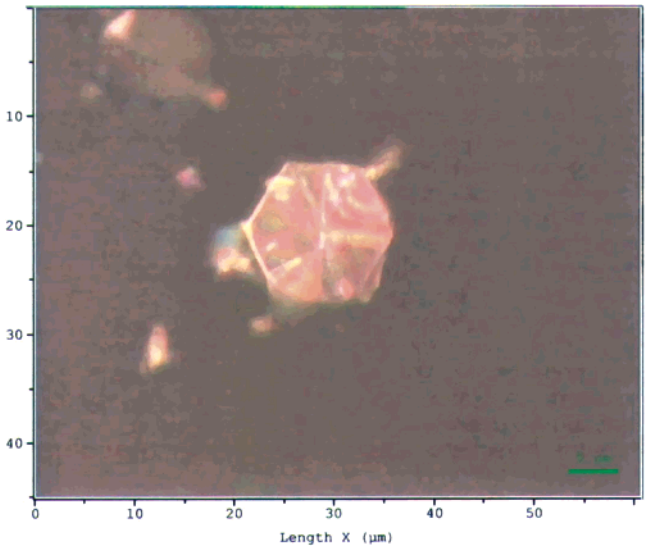

Figure 13. Photography of a crystal of the $CDCl_3$−cryptophane-E complex.

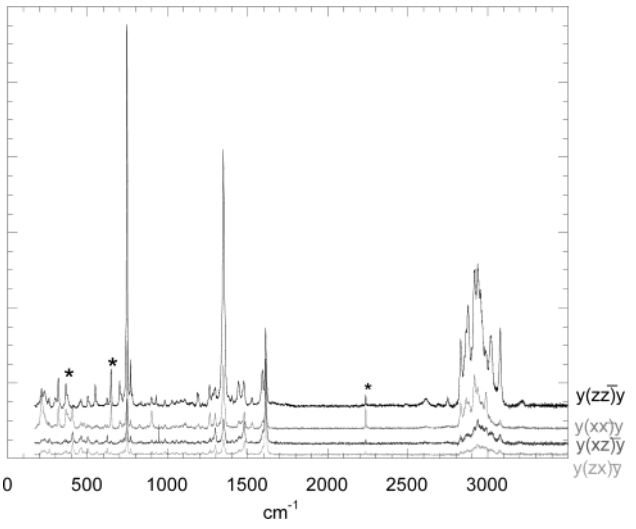

Figure 14. $y(xx)\bar{y}$, $y(zz)\bar{y}$, $y(xz)\bar{y}$, and $y(zx)\bar{y}$ Raman spectra of a crystal of the $CDCl_3$−cryptophane-E complex. $CDCl_3$ bands are noted with an asterisk.

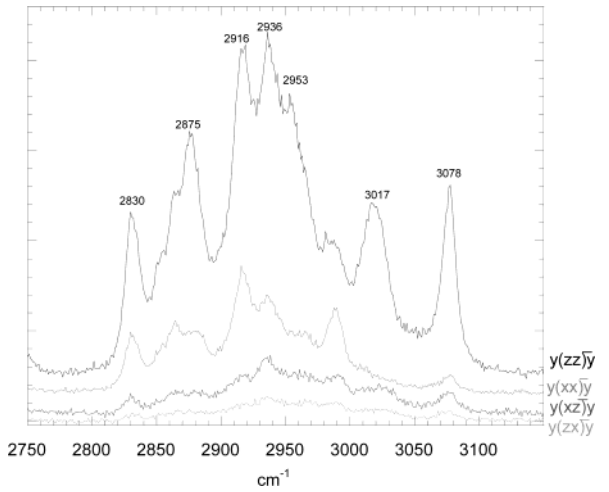

Figure 15. $y(xx)\bar{y}$, $y(zz)\bar{y}$, $y(xz)\bar{y}$, and $y(zx)\bar{y}$ Raman spectra of a crystal of the $CDCl_3$−cryptophane-E complex in the CH stretching region.

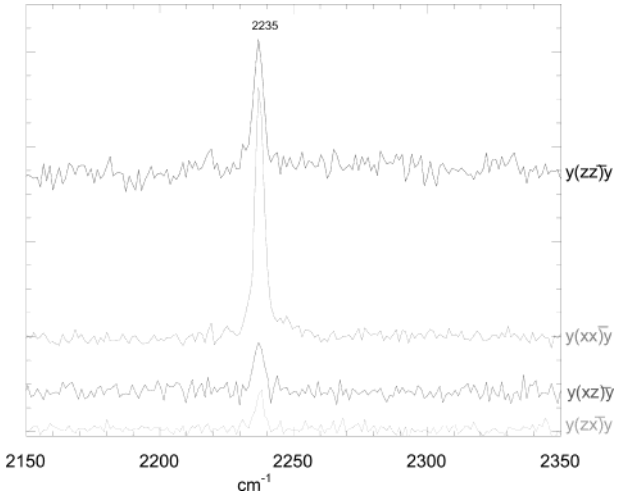

Figure 16. $y(xx)\bar{y}$, $y(zz)\bar{y}$, $y(xz)\bar{y}$, and $y(zx)\bar{y}$ Raman spectra of a crystal of the $CDCl_3$−cryptophane-E complex in the CD stretching region.

suggests that the motion of the chloroform molecules inside cage E (volume of the cavity ≈ 104 Å^3) is less hindered than in cage A (volume of the cavity ≈ 82 Å^3).

These data nicely confirm our NMR results performed on both complexes, which show a better affinity of the chloroform for cryptophane-E than for cryptophane-A.[33]

Conclusions

In this paper,we have demonstrated through the study of $CDCl_3$−cryptophane model systems the ability of Raman microspectrometry to investigate molecular recognition phenomena in solids. Indeed, the νC−D stretching vibration of the guest chloroform is a powerful IR and Raman spectroscopy probe and is very sensitive to small changes in the surrounding environment. This νC−D stretching band exhibits a significant red shift when the guest is encaged in both cryptophane-A and -E compared to its corresponding wavenumber in the gas phase (Table 2). This shift is larger for $CDCl_3$−cryptophane-E (30 ± 2 cm^{-1}) than for $CDCl_3$−cryptophane-A (20 ± 2 cm^{-1}). This softening of the CD stretching mode is characteristic of a specific proton donor−acceptor interaction between the C−D bond and the cryptophane cavity, which is stronger with cryptophane-E than with cryptophane-A. This difference can be related to the NMR results showing a better affinity of the chloroform for cryptophane-E than for cryptophane-A.

The differences observed in the CD stretching band shapes for the $CDCl_3$−cryptophane-E and $CDCl_3$−cryptophane-A complexes also suggest that the internal rotational dynamics of the guest molecules is different in each cavity.

The high sensitivity of this Raman microspectrometry technique allows us to distinguish between the two common polymorph structures of $CDCl_3$−cryptophane-A complexes. In the Raman spectra of the rod crystals, the presence of a second νCD band at higher frequency than that corresponding to the encaged chloroform molecule is related to the interstitial chloroform molecules present in the crystal lattice. The temperature dependence of the νCD stretching vibrations of the chloroform suggests that the motion of the encaged chloroform is more hindered than that of the interstitial chloroform.

To our knowledge, Raman microspectrometry has never been employed to investigate host−guest systems. The use of this technique seems promising because of its sensitivity, its rapidity, and its selectivity. Indeed, we can analyze small samples (a few dozen of μm^2), and the Raman spectra of selectively chosen microcrystals can be recorded in a few minutes, which is crucial for metastable crystals. Furthermore, polarized Raman spectrometry is a powerful tool for the characterization of the orientation of encaged chloroform molecules. The ability of Raman spectrometry to extract useful information about host−guest systems in solids makes this technique very attractive for organic chemists working in the field of supramolecular chemistry and represents a complementary tool to NMR spectroscopy for investigating host−guest systems.

When optical axes can be determined, as illustrated by the rhomb crystals study, Raman microspectrometry is sufficient to determine the guest orientation in the cryptophane host, the X-ray structure confirming this result.

Finally, the synthesis of a fully deuterated cryptophane would be useful in studying molecular recognition between chloroform or dichloromethane and cryptophanes and would significantly enhance the sensitivity of the technique. In addition, it represents an interesting challenge in cryptophane chemistry.

Acknowledgment. Y. Danten is gratefully acknowledged for useful discussions in ab initio calculations elaboration. We also thank M. Couzi for fruitful discussions and D. Talaga for experimental assistance.

References and Notes

(1) Collet, A. In *Comprehensive Supramolecular Chemistry*; Atwood, J. L., Davis, J. E. D., MacNicol, D. D., Vögtle, F., Eds.; Pergamon Press: New York, 1996; Vol. 2, Chapter 11, pp 325−365.

(2) Canceill, J.; Césario, M.; Collet, A.; Guilhem, J.; Lacombe, L.; Lozach, B.; Pascard, C. *Angew. Chem., Int. Ed. Engl.* **1989**, *28*, 1246.

(3) Garel, L.; Dutasta, J. P.; Collet, A. *Angew. Chem., Int. Ed. Engl.* **1993**, *32*, 1169.

(4) Bartik, K.; Luhmer, M.; Dutasta, J. P.; Collet, A.; Reisse, J. *J. Am. Chem. Soc.* **1998**, *120*, 784.

(5) Luhmer, M.; Goodson, B. M.; Song, Y.-Q.; Laws, D. D.; Kaiser, L.; Cyrier, M. C.; Pines, A. *J. Am. Chem. Soc.* **1999**, *121*, 3502.

(6) Brotin, T.; Lesage, A.; Emsley, L.; Collet, A. *J. Am. Chem. Soc.* **2000**, *122*, 1171.

(7) Lang, J.; Dechter, J. J.; Effemey, M.; Kowalewski, J. *J. Am. Chem. Soc.* **2001**, *123*, 7852.

(8) Tosner, Z.; Lang, J.; Sandström, D.; Petrov, O.; Kowalewski, J. *J. Phys. Chem. A* **2002**, *106*, 8870.

(9) Davidson, A. M.; Mellot, C. F.; Eckert, J.; Cheetham, A. K. *J. Phys. Chem. B* **2000**, *104*, 432. Mellot, C. F.; Davidson, A. M.; Eckert, J.; Cheetham, A. K. *J. Phys. Chem. B* **1998**, *102*, 2530.

(10) Bosch, E.; Huber, S.; Weitkamp, J.; Knozinger, H. *Phys. Chem. Chem. Phys.* **1999**, *4*, 579.

(11) *Comprehensive Supramolecular Chemistry*; Atwood, J. L., Davies, J. E., MacNicol, D. D., Vögtle, F., Eds.; Pergamon Press: New York, 1996; Vol. 8, Chapter 2, pp 33−120.

(12) *Raman Microscopy: Developments and Applications*; Turrell, G., Corset, J., Eds.; Academic Press: London, 1996.

(13) Baldwin, K. J.; Batcheler, D. N.; Webster, S. In *Handbook of Raman Spectroscopy*; Lewis, I. R., Edwards, H. G. M., Eds.; Marcel Dekker: New York, 2001; pp 145−190.

(14) McKean, D. C. *J. Mol. Struct.* **1984**, *113*, 251.

(15) Gorse, D.; Cavagnat, D.; Pesquer, M.; Lapouge, C. *J. Phys. Chem.* **1996**, *97*, 4262.

(16) Lapouge, C.; Cavagnat, D. *J. Phys. Chem. A* **1998**, *102*, 8393.

(17) Canceill, J.; Collet, A.; Gottarelli, G.; Palmieri, P. *J. Am. Chem. Soc.* **1987**, *109*, 6454.

(18) Brotin, T.; Devic, T.; Lesage, A.; Emsley, L.; Collet, A. *Chem.−Eur. J.* **2001**, *7*, 1561.

(19) Darzac, M.; Brotin, T.; Bouchu, D.; Dutasta, J. P. *Chem. Commun.* **2002**, 48.

(20) Darzac, M.; Brotin, T.; Rousset-Azrel, L.; Bouchu, D.; Dutasta, J. P. *New J. Chem.* 2004, in press.

(21) Sheldrick, G. M. *SHELXS-97: A Program for Crystal Structure Solution* and *SHELXL-97: A Program for Refinement of Crystal Structure*; University of Göttingen: Göttingen, Germany, 1997.

(22) Damen, T. C.; Porto, S. P. S.; Tell, B. *Phys. Rev.* **1966**, *142*, 570.

(23) Sears, D. N.; Jameson, C. J. *J. Chem. Phys.* **2003**, *119*, 12231.

(24) Frisch, M. J.; Trucks, G. W.; Schlegel, H. B.; Scuseria, G. E.; Robb, M. A.; Cheeseman, J. R.; Zakrzewski, V. G.; Montgomery, J. A., Jr.; Stratmann, R. E.; Burant, J. C.; Dapprich, S.; Millam, J. M.; Daniels, A. D.; Kudin, K. N.; Strain, M. C.; Farkas, O.; Tomasi, J.; Barone, V.; Cossi,

M.; Cammi, R.; Mennucci, B.; Pomelli, C.; Adamo, C.; Clifford, S.; Ochterski, J.; Petersson, G. A.; Ayala, P. Y.; Cui, Q.; Morokuma, K.; Malick, D. K.; Rabuck, A. D.; Raghavachari, K.; Foresman, J. B.; Cioslowski, J.; Ortiz, J. V.; Stefanov, B. B.; Liu, G.; Liashenko, A.; Piskorz, P.; Komaromi, I.; Gomperts, R.; Martin, R. L.; Fox, D. J.; Keith, T.; Al-Laham, M. A.; Peng, C. Y.; Nanayakkara, A.; Gonzalez, C.; Challacombe, M.; Gill, P. M. W.; Johnson, B. G.; Chen, W.; Wong, M. W.; Andres, J. L.; Head-Gordon, M.; Replogle, E. S.; Pople, J. A. *Gaussian 98*, revision A; Gaussian, Inc.: Pittsburgh, PA, 1998.

(25) Biarge, J. F.; Herrantz, J.; Morcillo, J. *J. Annu. Rev. Soc. Esp. Fis. Quim.* **1961**, A57.

(26) Person, W. B.; Newton, J. H. *J. Chem. Phys.* **1974**, *61*, 1040.

(27) Cavagnat, D.; Danten, Y.; Guillaume, F. To be submitted for publication.

(28) *Raman/Infrared Atlas of Organic Compounds*, 2nd ed.; Schrader, B., Ed.; VCH: Weinheim, Germany, 1989. Bermejo, D.; Escribano, R.; Orza, J. M. *J. Raman Spectrosc.* **1977**, *8*, 151. Ruoff, A.; Burger, H. *Spectrochim. Acta A* **1970**, *26*, 989. Schmidt, K. H.; Müller, A. *J. Mol. Spectrosc*. **1974**, *50*, 115.

(29) Nomura, H.; Koda, S.; Miyahara, Y. *J. Chem. Phys.* **1976**, *11*, 4339.

(30) Jemmis, E. D.; Giju, K. T.; Sundararajan, K.; Sankaran, K.; Vidya, V.; Viswanathan, K. S.; Lesszczynski, J. *J. Mol. Struct.* **1999**, *510*, 59. Danten, Y.; Tassaing, T.; Besnard, M. *J. Phys. Chem. A* **2000**, *104*, 9415. Raveendran, P.; Wallen, S. L. *J. Am. Chem. Soc.* **2002**, *124*, 12590.

(31) Gellini, C.; Moroni, L.; Munoz-Miranda, M. *J. Chem. Phys. A* **2002**, *106*, 10999.

(32) Ramana Rao, P. V.; Ramana Rao, G. *Spectrochim. Acta, Part A* **2002**, *58*, 3039.

(33) Collet, A.; Dutasta, J.-P.; Lozach, B.; Canceill, J. *Top. Curr. Chem.* **1993**, *165*, 103−129.